UNIVERSITY OF CAMBRIDGE

Flow Field Results of the Cambridge Stratified Swirl Burner Using Laser Doppler Anemometer

Technical Report CUED/A-TURBO/TR.134

R. Zhou*, M.S. Sweeney, S. Hochgreb

Cambridge Combustion Research Centre

Department of Engineering, University of Cambridge

*rz242@cam.ac.uk

Abstract

A series of flow fields generated by a turbulent methane/air stratified swirl burner are investigated using laser Doppler anemometer (LDA) to obtain the velocities in axial, radial and tangential directions. The experimental methodology, data processing routines and the data format are detailed in this report.

1. Experimental Details

An overview of the swirl burner, operating conditions, and experimental methods used is provided to give context to the results presented further on in the present work.

1.1. Cambridge Stratified Swirl Burner

The burner was designed by Mark Sweeney at Cambridge University and has been used for advanced scalars measurements in Sandia National Laboratory to provide validation cases for modellers [1-3]. This burner provides flows with a variable degree of swirl; this was to approximate the flow conditions found in many practical applications, and to introduce a greater degree of complexity to the test case. The swirl assists flame stabilization, as in practical combustors, allowing more extreme stratified conditions to be investigated than would otherwise be possible. The swirl burner is referred to as *Sw*B throughout the present work.

The swirl burner is shown in Figure 1; key components are labelled and are referenced in braces, {}, in the following discussion. It consists of two annular channels through which fuel/oxidizer mixtures can flow, and a large (382 mm diameter) co-flow of filtered air to prevent the entrainment of ambient air. Air flow in the co-flow is conditioned in the following way. First, it is passed through 3 perforated disks {M}, the first of which has 3 mm diameter holes with 40% open area, while the subsequent pair has 1.5 mm diameter holes with 25% open area. The flow is then straightened by passing it through a 38.1 mm deep honeycomb section {L} with 3 mm holes and 75% open area. Finally any clustered particles are filtered using two mesh gauzes {K}, the first of which has 1.2 mm square holes and 70% open area, while the second has 1 mm square holes with 40% open area.

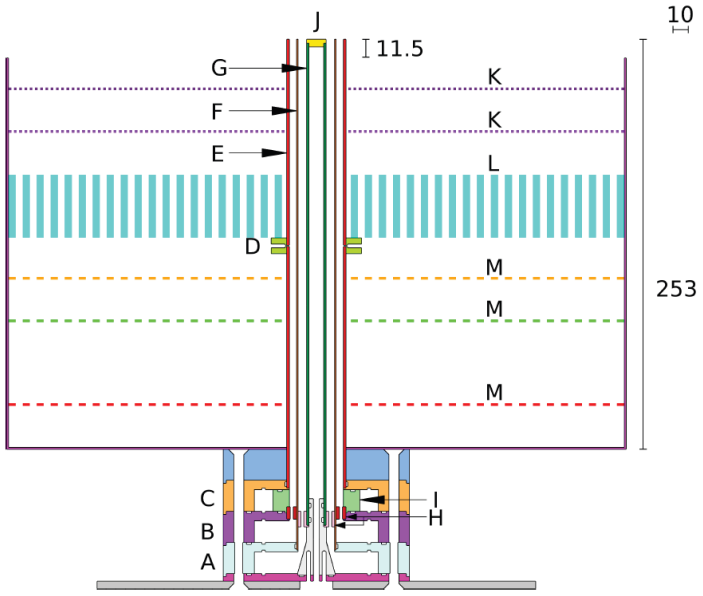

Figure 1: Elevation of the stratified swirl burner (*Sw*B). A: inner annulus plenum; B: outer annulus axial flow plenum; C: outer annulus swirl flow plenum; D: locating collar; E: outer tube; F: middle tube; G: inner tube; H: flow straighteners; I: swirl generating collar; J: ceramic cap; K: wire mesh; L: honeycomb section; M: perforated disk. Flow fittings are omitted for clarity. All dimensions are to scale and in mm.

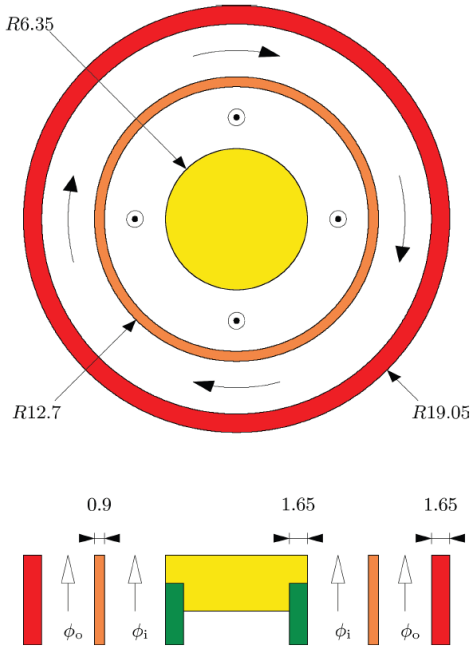

Figure 2: Plan view schematic of the exit geometry in the stratified swirl burner (*Sw*B), showing a plan view and a cross section through the burner axis. The curved vectors in the plan view show the direction of swirling flows in the outer annulus, while the out of page vectors show the axial flow in the inner annulus. All dimensions are to scale and in mm.

The annuli are formed by three concentric tubes {E-G}. The exit geometry is shown in Figure 2. The innermost tube {G} is terminated in a ceramic cap {J}. This acts as a central bluff body which aids flame stabilization. The use of ceramic material ensures that heat losses to the bluff body are minimized, and the conditions are assumed to be close to adiabatic. Furthermore, the ceramic used is essentially an inert material in comparison to alternatives such as stainless steel, with the result radical absorption and surface reactions are minimized.

A locating collar {D} is used to ensure that the major axes of the tubes are coincident. The outer tube {E} is aligned relative to the middle tube {F} using a set of three 0.6 mm diameter pins arranged at 120˚. The diameter of the pins was selected as a compromise between structural strength and the desire to minimize disturbance to the flow.

The perturbation of the flow was further reduced by placing the locating collar 133 mm upstream of the burner exit. The pins are slotted through holes in the locating collar and the outer tube, and the relative position of the middle tube is controlled by varying the depth to which the pins are screwed into the locating collar. A transparent alignment mask with concentric markings corresponding to the desired positions of the various tubes was placed on the outer tube to assist location. Annular gap widths were uniform to within approximately 0.05 mm. Another set of three pins, offset by 30˚ to the previously mentioned set, is used to locate the inner tube relative to the outer one following a similar procedure.

Flow to the inner annulus is supplied via a plenum {A} at the base of the burner, mixing of fuel and oxidizer gases having taken place in feed lines far upstream of the burner. Though the primary purpose of the plenum is to channel flow from the supply lines to the inner annulus, it also breaks up the flow structures in the lines on entrance to the burner. The outer annulus is fed by the middle and upper plenums {B, C} in the burner. If the middle plenum {B} is used in isolation, then the resulting outer annulus flow is axial. A variable degree of swirl can be introduced to the outer flow by passing a percentage of the overall outer annulus flow through upper plenum {C}. Gas from the upper plenum joins the outer annulus through a swirl collar {I}, via a radially symmetric pattern of inlets angled at 30˚ to the annulus and at 30˚ to the horizontal. These angled jets induce a tangential component to the axial flow from the middle plenum, generating a swirling flow at the burner mouth.

Flow straightening rings {H} are fitted to the inner and outer annulus close to the plenums supplying axial flow. The rings have a number of small through-holes arranged in a radially symmetric pattern, with major axes parallel to those of the annuli. Turbulence is generated by the

changes in sectional area as flow passes through the holes, and the pressure drop across them is sufficiently high to ensure uniform flow.

The distance between the flow straighteners and the burner exit is a compromise between the need for a long axial length to ensure that turbulence is fully developed, the practical challenges long burner geometries pose for laser diagnostics, and the decay of swirl and turbulence intensity with distance. The development length is over 25 diameters in each annulus, which is sufficient to give well developed turbulent flow at exit for this compact burner geometry. The development length is also short enough to avoid excessive decay of swirl (used in subsequent experiments) before reaching the burner exit. Detailed drawings are available online [7].

1.2. Operating Conditions

The LDA measurements were taken in reacting and non-reacting conditions under three levels of swirl - nonswirling, moderately swirling and highly swirling. These cases correspond to the reacting cases investigated using scalar measurements in previous publications by this group [1-3]. Throughout the present work, non-reacting flows are denoted by the prefix *c* — e.g. *cSw*B1 refers to the non-swirling non-reacting flow, whereas *Sw*B1 refers to non-swirling non-reacting flow.

The bulk velocity in the outer annulus, U_o = 18.7 m/s, was set at more than twice the value of the velocity in the inner annulus, U_i = 8.3 m/s, in order to generate substantial levels of shear between the two flows. Co-flow air was supplied around the outer annulus with a bulk velocity $U_{co\text{-}flow}$ = 0.4 m/s to prevent the entrainment of ambient air. The Reynolds numbers ($Re = \rho UL/\mu$) derived from the bulk velocities and the exit geometry are Re_i = 5960 for the inner annulus and Re_o = 11500 for the outer annulus.

The swirl flow ratio, SFR, defined as the ratio of outer annulus flow through the swirl plenum to that through the axial plenum, was varied between 0 for non-swirling flow to 0.4 for very highly swirling flow. The highly stratified 0.4 swirl flow ratio cases did not stabilize reliably; the high strain at the flame base made the flame liable to detach and blow off. The SFR = 0.4 cases were not measured during experimental campaigns because of this tendency to blow off.

Table 1 below listed the operating conditions for reacting and non-reacting cases of the burner.

Table 1: Operating conditions for reacting and non-reacting cases. The gas flows in all experiments were metered using mass flow controllers. All the controllers used for the velocity characterization were Alicat mass flow controllers and unit for the flow rate is SLPM. Φ_g: global equivalence ratio; Φ_i: equivalence ratio in the inner annulus; Φ_o: equivalence ratio in the outer annulus; SR: stratification ratio; SFR: swirl flow ratio. Outer Main: refers to flow through {B}; Outer Swirl: refers to flow through {C}; Inner: refers to flow through {A}.

						Outer Main		Outer Swirl		Inner		Coflow
Case	Φ_g	SR	Φ_i	Φ_o	SFR	Air	CH4	Air	CH4	Air	CH4	Air
*Sw*B1	0.75	1.00	0.75	0.75	0.00	441.70	34.80	0.00	0.00	144.00	11.35	765.60
*Sw*B2	0.75	1.00	0.75	0.75	0.25	331.28	26.10	110.43	8.70	144.00	11.35	765.60
*Sw*B3	0.75	1.00	0.75	0.75	0.33	295.94	23.32	145.76	11.48	144.00	11.35	765.60
*Sw*B4	0.75	1.00	0.75	0.75	0.40	265.02	20.88	176.68	13.92	144.00	11.35	765.60
*Sw*B5	0.75	2.00	1.00	0.50	0.00	452.70	23.80	0.00	0.00	140.60	14.77	765.60
*Sw*B6	0.75	2.00	1.00	0.50	0.25	339.53	17.85	113.18	5.95	140.60	14.77	765.60
*Sw*B7	0.75	2.00	1.00	0.50	0.33	303.31	15.95	149.39	7.85	140.60	14.77	765.60
*Sw*B8	0.75	2.00	1.00	0.50	0.40	271.62	14.28	181.08	9.52	140.60	14.77	765.60
*Sw*B9	0.75	3.00	1.13	0.38	0.00	458.40	18.10	0.00	0.00	139.00	16.42	765.60
*Sw*B10	0.75	3.00	1.13	0.38	0.25	343.80	13.58	114.60	4.53	139.00	16.42	765.60
*Sw*B11	0.75	3.00	1.13	0.38	0.33	307.13	12.13	151.27	5.97	139.00	16.42	765.60
*Sw*B12	0.75	3.00	1.13	0.38	0.40	275.04	10.86	183.36	7.24	139.00	16.42	765.60
*cSw*B1	-	-	-	-	0.00	476.5	0.00	0.00	0.00	155.35	0.00	765.60
*cSw*B2	-	-	-	-	0.25	357.38	0.00	119.13	0.00	155.35	0.00	765.60
*cSw*B3	-	-	-	-	0.33	319.26	0.00	157.25	0.00	155.35	0.00	765.60

1.3 LDA set up

The LDA system consists of a continuous laser, a transmitter, an emitter and a receiver. The laser used is an Ar-ion continuous laser (Spectra-Physics Stabilite 2017) operating at λ=514.5 nm and 488 nm with power set to 1.5 W. The integrated transmitter unit split the laser beam into two colour components with 514.5 nm and 488 nm wavelengths, and to divide each colour into two beams with a 40 MHz frequency difference. Two pairs of beams generated by the transmitter are emitted by an emitter with a 500 mm focal length lens in front. Resulted four beams cross at the focal point and form a measuring volume as shown in Figure 3a. The inner annulus, outer annulus, and co-flow of the burner were each seeded with 1 µm calcined aluminium oxide particles. The signals generated by the particles crossing the measuring volume were transferred to the BSA processor through a Nikon Micro Nikkor 105 mm 1:2.8D lens (f/2.8) and a Dantec colour separator and photodetectors operating at λ=514.5 and 488 nm. Figure 3b shows the LDA set up and side scattering configuration.

(a) (b)

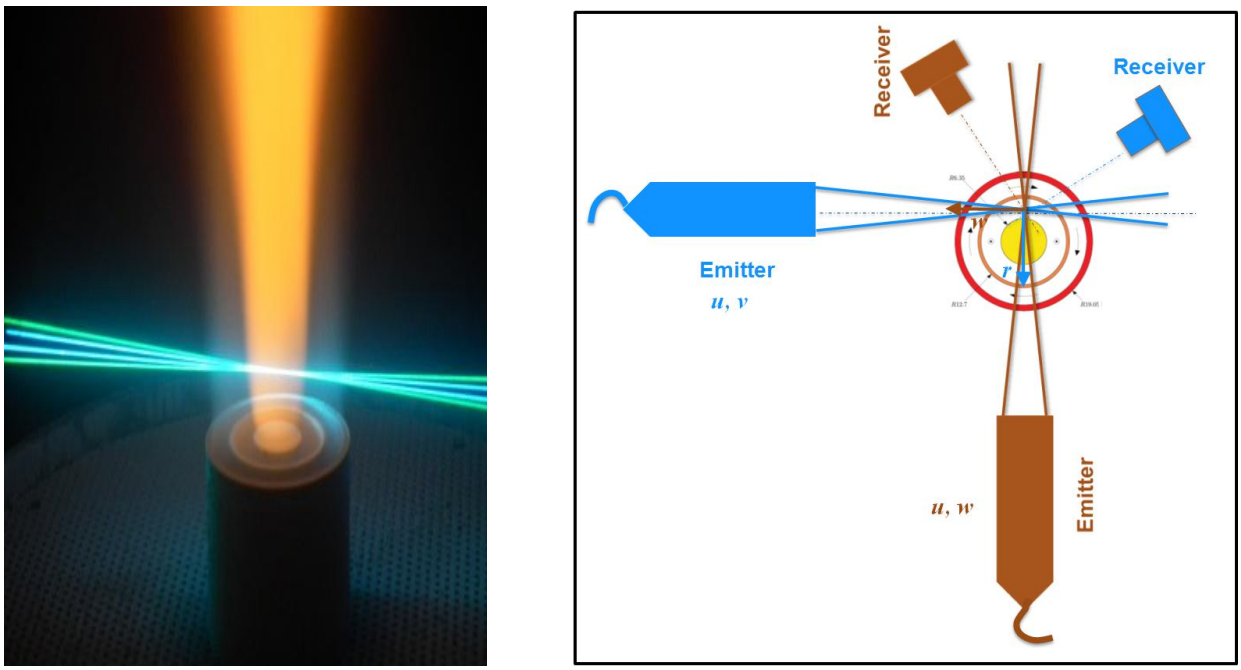

Figure 3. (a) LDA measurements in real world. (b) LDA set up and forward side scattering configuration. Note: the settings colored by blue are for axial *u* and radial velocity *v* components (UV), whereas the settings for axial *u* and tangential velocity *w* component (UW) were rotated 90˚ and shown in green. Both settings scanned along *r* on both sides of the burner.

Table 2 lists the resulted dimensions of the measuring volume and the approximated data rates for the measured velocity components. The bolded numbers refer to important resolutions for corresponding components.

The LDA measurements were done at different axial locations corresponding to those of the previous publications regarding the scalar measurements [1-3]. Table 3 lists the scanned cases and measured axial locations.

Table 2: Resolutions and data rates for measured velocity components.

Velocity component	Resolution in axial direction (mm)	Resolution in radial direction (mm)	Resolution in tangential direction (mm)	Data rate (Hz)
Axial u	**0.142**	0.142	3.461	~10 k
Radial v	0.135	**0.135**	3.365	~10 k
Tangential w	0.135	3.365	**0.135**	~10 k

Table 3: Cases surveyed by LDA at different axial locations. Note: flames were scanned on both sides of the burner.

Axial location (mm) / Case	2	10	30	40	50	70
*Sw*B1 (*u*, *v*, *w*)	√	√	√		√	√
*Sw*B2 (*u*, *v*, *w*)	√	√	√	√	√	
*Sw*B3 (*u*, *v*, *w*)	√	√	√		√	
*Sw*B5 (*u*, *v*, *w*)	√	√	√		√	√
*Sw*B6 (*u*, *v*, *w*)	√	√	√	√	√	
*Sw*B7 (*u*, *v*, *w*)	√	√	√		√	
*Sw*B9 (*u*, *v*, *w*)	√	√	√		√	√
*Sw*B10 (*u*, *v*, *w*)	√	√	√	√	√	
*Sw*B11 (*u*, *v*, *w*)	√	√	√		√	
*cSw*B1 (*u*, *v*, *w*)	√	√	√		√	
*cSw*B2 (*u*, *v*, *w*)	√	√	√		√	
cSwB3 (*u*, *v*, *w*)	√	√	√		√	

2. Data processing

The LDA measurements provide velocity results with high temporal resolution, enabling the power spectral analysis of the flow field. However, the present report focuses only on the calculations of the mean and RMS for the axial, radial and tangential velocity components. Readers interested in the turbulence spectra of the burner may refer to the technical report [4] by the same authors.

2.1 LDA signal processing parameters

The burst signals detected by the receiver were processed by the BSA processor [5]. Key parameters include Minimum record length, Maximum record length, High voltage level, Signal gain, Burst detector SNR level and Level validation ratio. These parameters were selected as a compromise between high data rate and high signal to noise ratio (SNR). Tests have been done to optimize these parameters and the resulted values are listed in Table 4.

Table 4: Signal processing parameters.

Case	Minimum record length	Maximum record length	High voltage level (V)	Signal gain (dB)	Burst detector SNR level (dB)	Level validation ratio
Non reacting	32	256	1200	24	5	4
Reacting	32	256	1600	24	5	4

2.2 Transit time weighting

During periods of higher velocity, a larger volume of fluid is swept through the measuring volume, and consequently a greater number of velocity samples will be recorded. As a direct result, an attempt to evaluate the statistics of the flow field using arithmetic averaging will bias the results in favor of the higher velocities. To correct this velocity-bias, a non-uniform weighting factor η_i is introduced.

$$\eta_i = \frac{t_i}{\sum_{j=0}^{j=N-1} t_j} \quad (1)$$

-where t_i is the transit time or residence time of the i'th particle crossing the measurement volume. Calculations of moments will use this weighting factor during averaging [5].

2.3 Mean and RMS Velocity

Mean and RMS of the axial, radial and tangential velocity components are calculated using the standard formula from the total set of N individual velocity samples.

Mean velocity:

$$u_{mean} = \sum_{i=0}^{N-1} \eta_i \; u_i \tag{2}$$

$$v_{mean} = \sum_{j=0}^{N-1} \eta_j \; v_j \tag{3}$$

$$w_{mean} = \sum_{k=0}^{N-1} \eta_k \; w_k \tag{4}$$

RMS velocity:

$$u_{RMS} = \sqrt{\sum_{i=0}^{N-1} \eta_i \; (u_i \; - u_{Mean})^2} \tag{5}$$

$$v_{RMS} = \sqrt{\sum_{j=0}^{N-1} \eta_j \; (v_j \; - v_{Mean})^2} \tag{6}$$

$$w_{RMS} = \sqrt{\sum_{k=0}^{N-1} \eta_k \; (w_k \; - w_{Mean})^2} \tag{7}$$

3. Results

The LDA data were examined in subsection 3.1 and 3.2 and preliminary results for all reacting and non reacting cases were shown in subsection 3.3.

3.1 LDA self-validation

The tangential and the radial velocity components were not obtained simultaneously. However, axial velocity components were measured twice as shown in Figure 3b (one with radial component and the other one with tangential component). Comparisons between these two sets of axial velocity component were made for all reacting cases at axial location *z*=30 mm (where the flame crosses the mixing layer according to the scalar measurements). Figure 4 shows that the axial velocity components from UV and UW measurements match very well with each other, which means that the measurements are highly repeatable even if they are not simultaneous, and the misalignments of UV and UW were negligible.

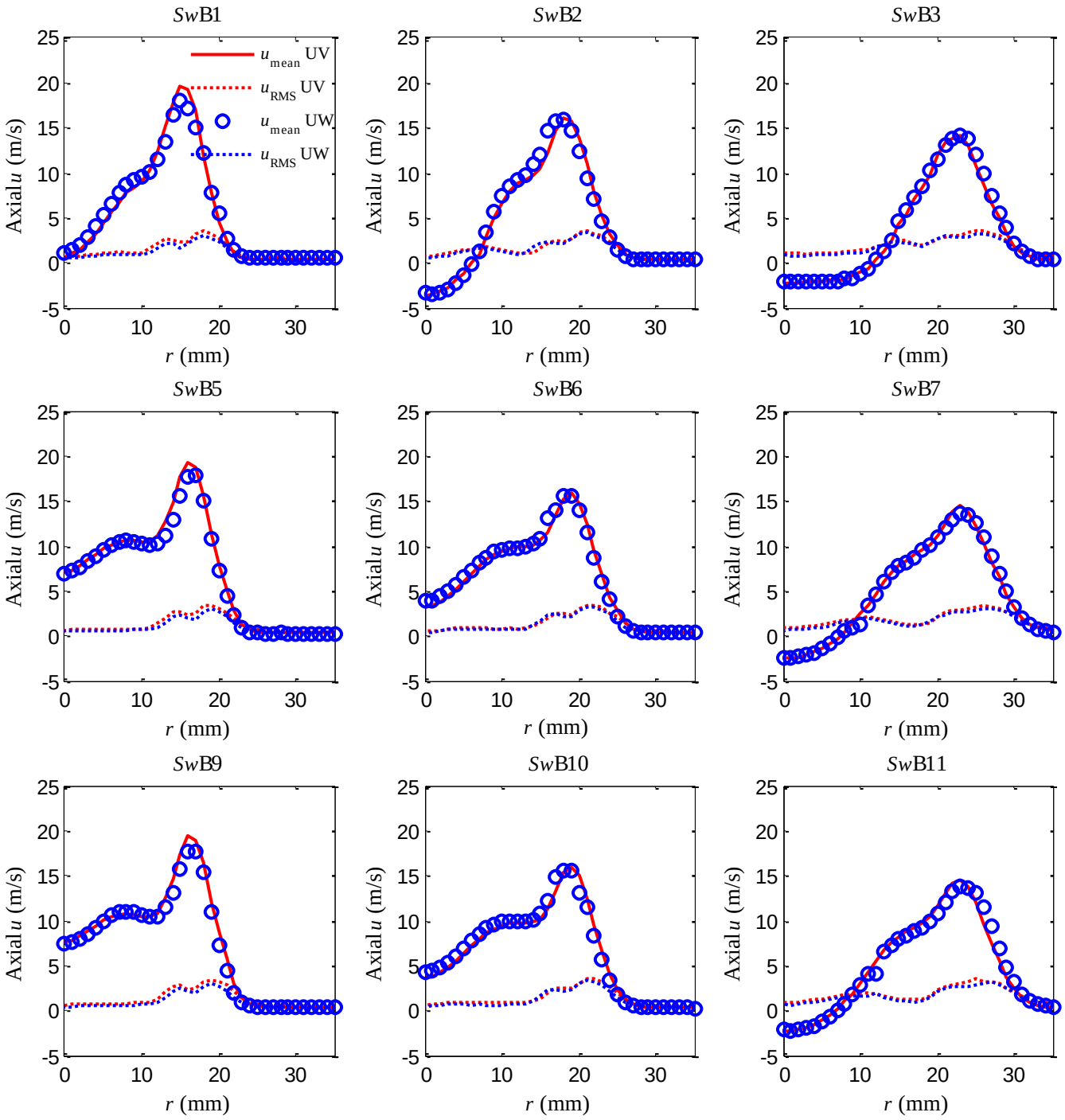

Figure 4. Mean and RMS for axial velocity components of all reacting cases at axial location z=30 mm obtained by LDA_UV and LDA_UW settings.

3.2 LDA vs PIV: non reacting cases

Axial and radial velocity components for non-reacting cases of the burner have been obtained using two-component PIV [6]. A preliminary comparison between the LDA and PIV results in the axial *u* velocity component is shown in Figure 5.

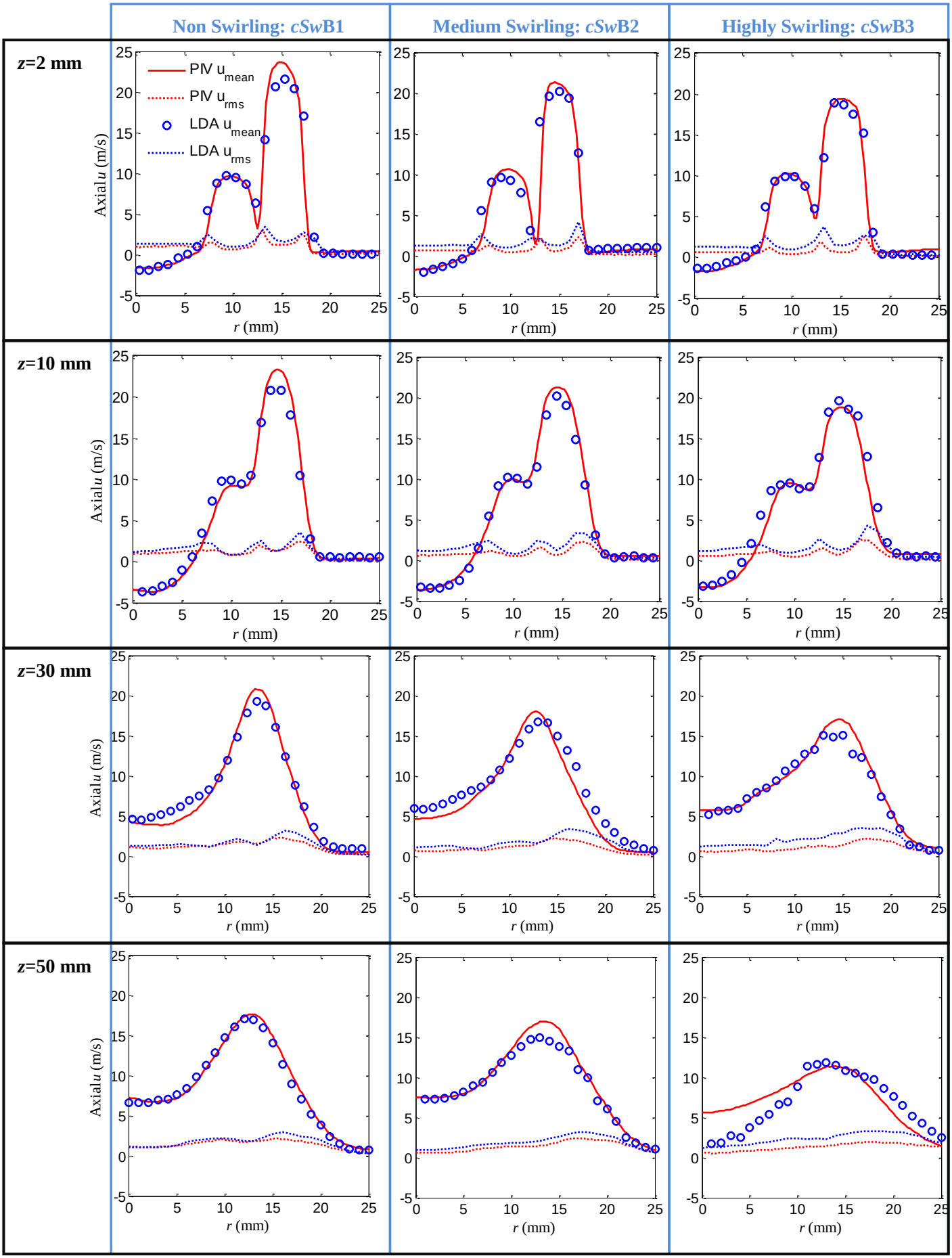

Figure 5. Mean and RMS for axial velocity components obtained by LDA and PIV under non reacting conditions.

3.3 LDA:Reacting vs Non Reacting

The data attached has been validated in subsection 3.1 and 3.2. In this subsection, profiles of mean and RMS for *u, v,* and *w* were extracted at different axial locations for all reacting and non reacting cases.

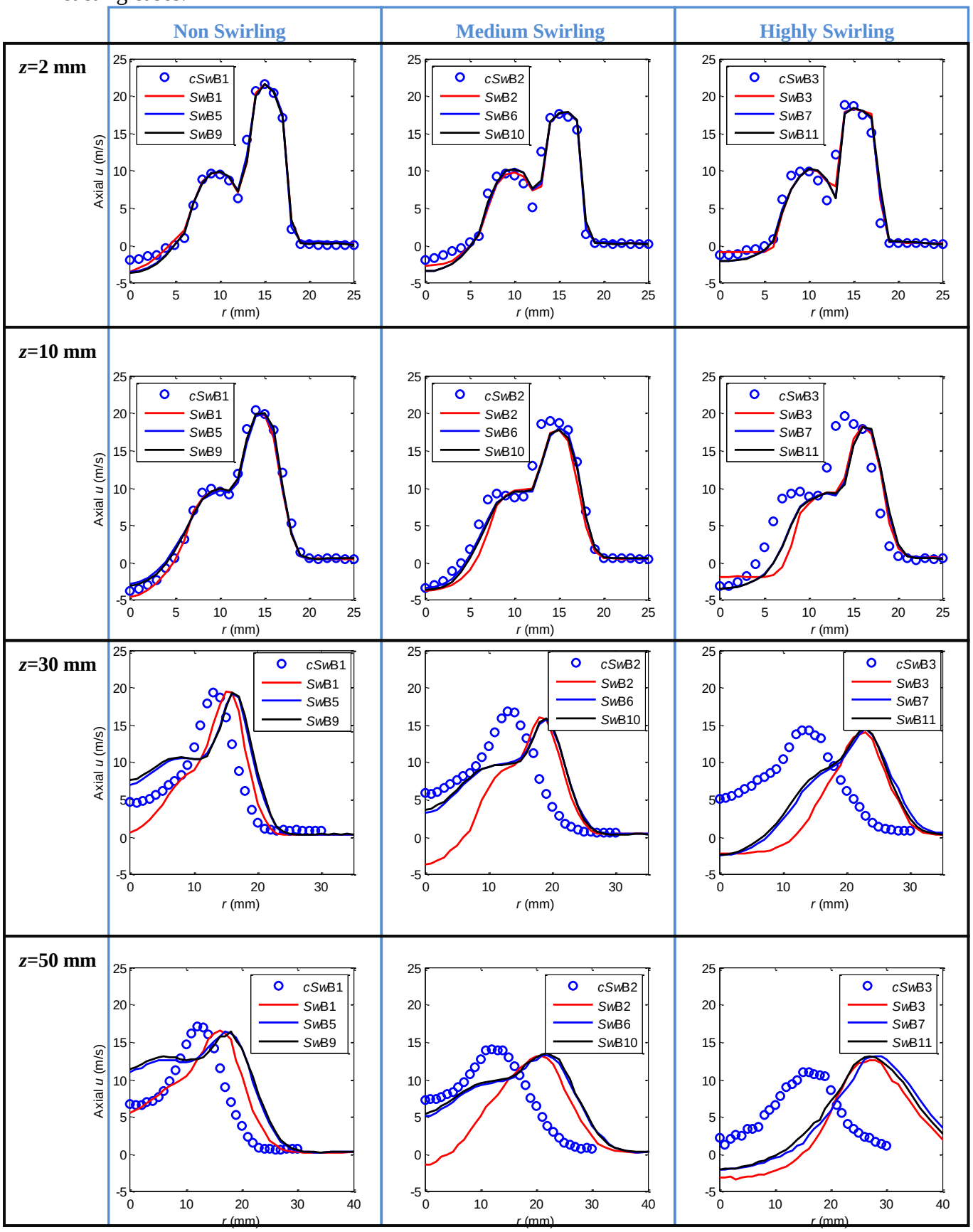

Figure 6. Mean for axial velocity components.

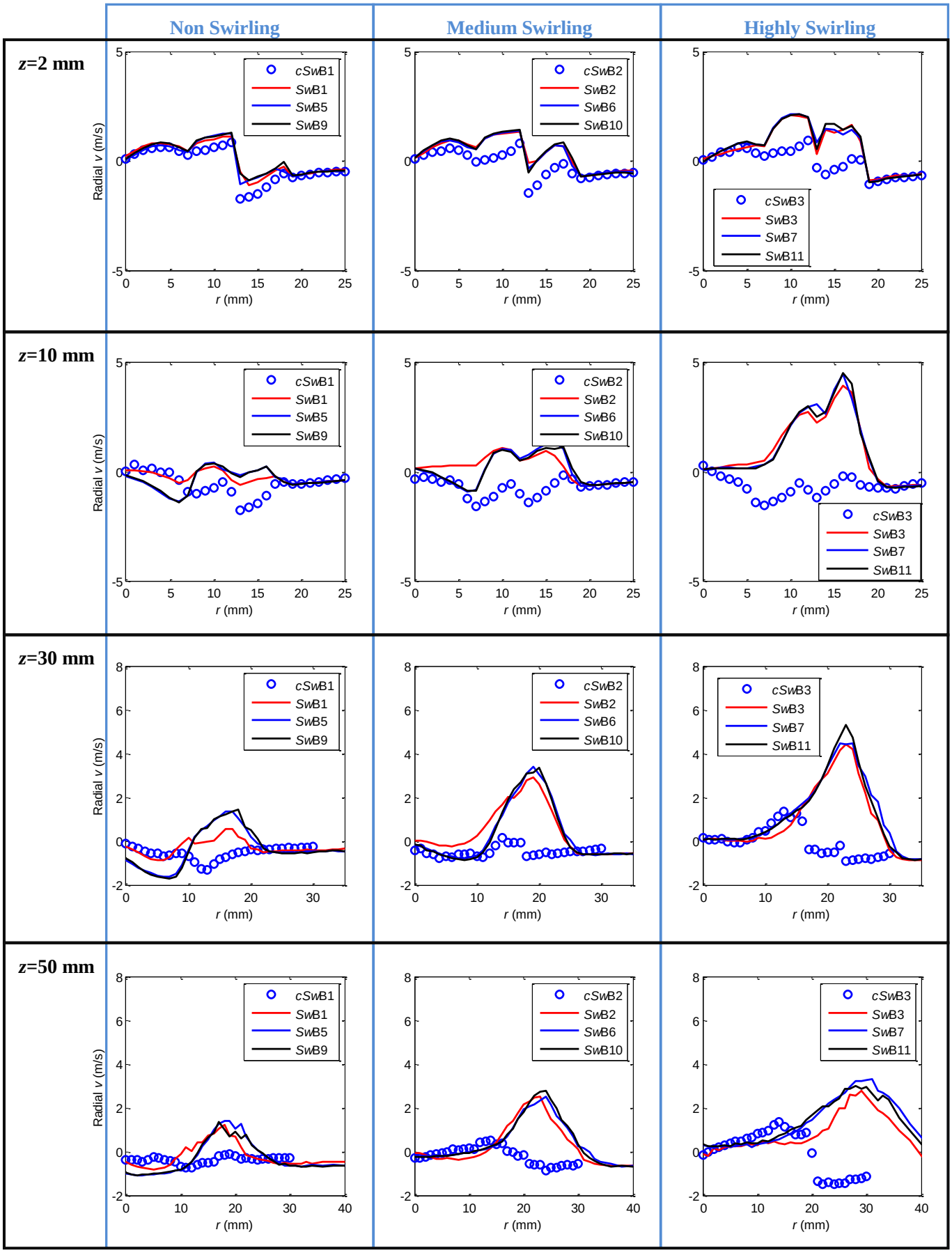

Figure 7. Mean for radial velocity components.

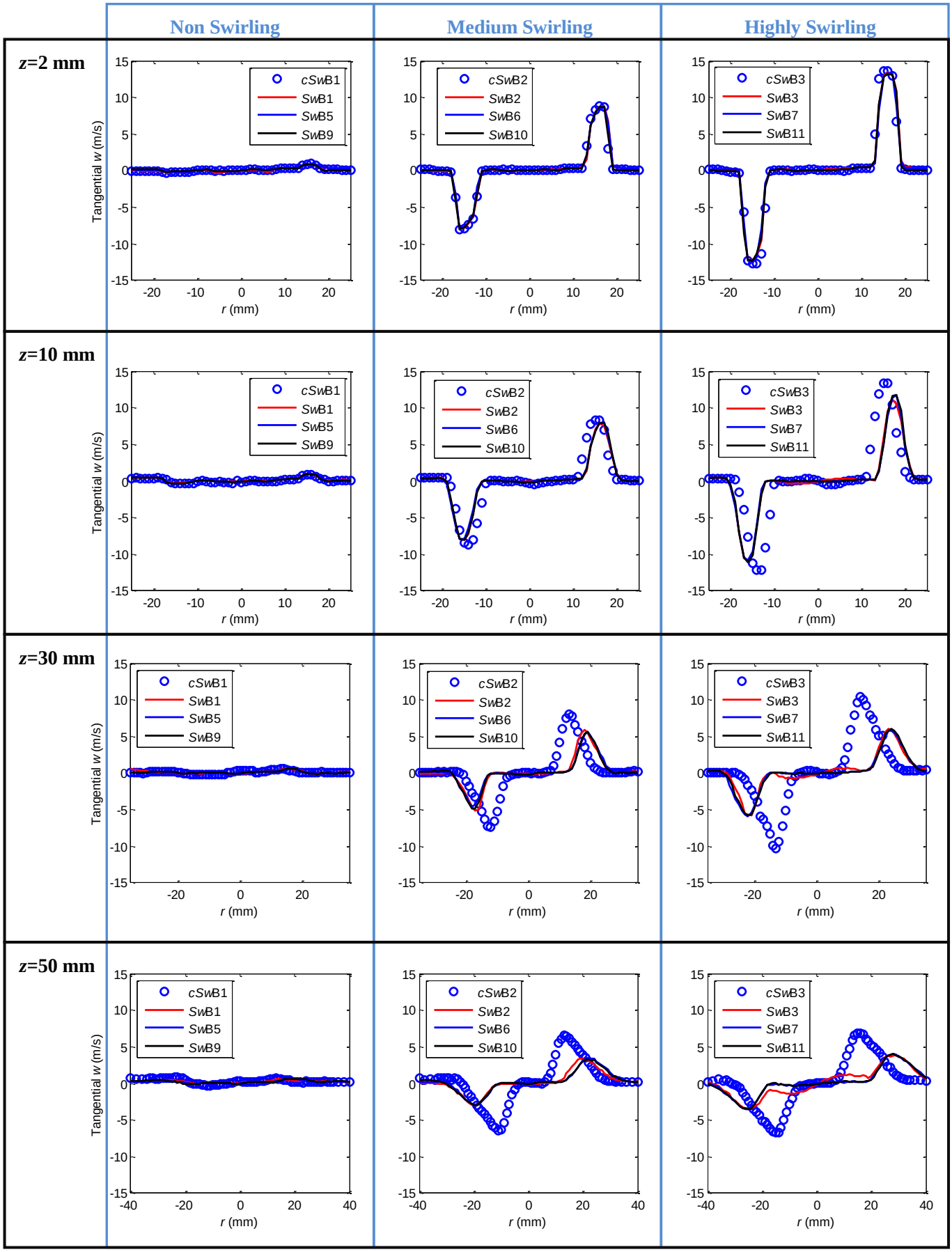

Figure 8. Mean for tangential velocity components.

4. Data format

All mean and RMS for the LDA results are stored in txt files [8]. Examples:

1) **For reacting cases:**
    a. **SwB1_z2_UV_MeanAndRMS.txt** corresponds to the mean and RMS of axial *u* and radial *v* velocity components for case *Sw*B1 at axial location 2 mm.

    Data structure:

    First column: Radial position (mm);

    Second column: Axial position (mm);

    Third column: Mean of the axial velocity (m/s);

    Fourth column: RMS of the axial velocity (m/s);

    Fifth column: Mean of the radial velocity (m/s);

    Sixth column: RMS of the radial velocity (m/s)

    b. **SwB1_z2_W_MeanAndRMS.txt** corresponds to the mean and RMS of tangential *w* velocity components for case *Sw*B1 at axial location 2 mm.

    Data structure:

    First column: Radial position (mm);

    Second column: Axial position (mm);

    Third column: Mean of the tangential velocity (m/s);

    Fourth column: RMS of the tangential velocity (m/s)

2) **For Non-reacting cases:**
    a. **cSwB1_ns_z2_UV_MeanAndRMS.txt** corresponds to the mean and RMS of axial *u* and radial *v* velocity components for **n**on-**s**wirling case *cSw*B1 at axial location 2 mm. **ns**: non-swirling, **ms**: medium swirling, **hs**: highly swirling.

    Data structure:

    First column: Radial position (mm);

    Second column: Axial position (mm);

    Third column: Mean of the axial velocity (m/s);

    Fourth column: RMS of the axial velocity (m/s);

    Fifth column: Mean of the radial velocity (m/s);

    Sixth column: RMS of the radial velocity (m/s)

b. **cSwB1_ns_z2_W_MeanAndRMS.txt** corresponds to the mean and RMS of tangential *w* velocity components for **n**on-**s**wirling case *cSw*B1 at axial location 2 mm.

Data structure:

First column: Radial position (mm);

Second column: Axial position (mm);

Third column: Mean of the tangential velocity (m/s);

Fourth column: RMS of the tangential velocity (m/s)

5. Reference

[1] M. S. Sweeney, S. Hochgreb, M. J. Dunn, R. S. Barlow, *The Structure of Turbulent Stratified and Premixed Methane/Air Flames I: Non-Swirling Flows*. Combustion and flame, in press, 2012.

[2] M. S. Sweeney, S. Hochgreb, M. J. Dunn, R. S. Barlow, *The Structure of Turbulent Stratified and Premixed Methane/Air Flames II: Swirling Flows*. Combustion and Flame, in press, 2012.

[3] M. S. Sweeney, S. Hochgreb, M. J. Dunn, R. S. Barlow, *A comparative analysis of flame surface density metrics in premixed and stratified flames.* Proceedings of the Combustion Institute 33 (2011). pp. 1419-1427. ISSN 1540-7489.

[4] R. Zhou, S. Balusamy, S. Hochgreb. *A Tool for the Spectral Analysis of the Laser Doppler Anemometer Data of the Cambridge Stratified Swirl Burner*. Technical Report CUED/A-TURBO/TR.135.
URL: http://www.dspace.cam.ac.uk/handle/1810/226463 , 2012.

[5] Dantec Dynamics A/S. *BSA Flow Software* Version 4.10, 2006.

[6] M. S. Sweeney, R. Zhou, S. Hochgreb, M. J. Dunn, R. S. Barlow, *2D PIV in Non-Reacting Conditions in Cambridge Stratified Swirl Burner*. Department of Engineering, University of Cambridge, 2012.

[7] M. S. Sweeney, S. Hochgreb, R. S. Barlow, *Cambridge Stratified Swirl Burner Technical Drawings*, Online, URL: http://www.dspace.cam.ac.uk/handle/1810/241609, 2012.

[8] R. Zhou, M. S. Sweeney, S. Hochgreb. *Flow Field Results of the Cambridge Stratified Swirl Burner Using Laser Doppler Anemometer*, Online, URL: http://www.dspace.cam.ac.uk/handle/1810/226463, 2012.